Gravitional effects on bed load transport at low shields stress: experimental observations

Gravitational effects on bed load transport at low Shields stress: Experimental observations

S. Francalanci[1,2] and L. Solari[1]

Received 9 November 2005; revised 2 August 2006; accepted 3 November 2006; published 16 March 2007.

[1] In the present study we investigate the bed load transport mechanism due to the action of a free surface water flow when the transversal and longitudinal slopes of the bed are not negligible and in the case of low values of the applied Shields stress. Such a problem, which has been recently tackled by Parker et al. (2003) by means of a theoretical formulation, does not appear to be fully addressed in the literature from an experimental point of view. To this aim, average motion characteristics and transport dynamics of bed particles over an arbitrarily inclined nonerodible bed are studied by means of an experimental activity based on different techniques. A laser Doppler and an image-based technique are developed here and employed to study the average properties of saltating particles, while volumetric sampling is applied to estimate the average bed load transport intensity at equilibrium. Results show the intensity and direction of average particle velocity and average bed load transport as a function of the applied Shields stress for various bed inclinations. It appears that the intensity of bed load transport increases with the applied Shields stress much faster than predicted by the linear formulations on horizontal beds, while its direction may largely deviate from the direction of the applied shear stress at the bed when the bed is transversally tilted. Experimental results are compared with the theoretical results of Parker et al. (2003) and show a good agreement.

Citation: Francalanci, S., and L. Solari (2007), Gravitational effects on bed load transport at low Shields stress: Experimental observations, *Water Resour. Res.*, *43*, W03424, doi:10.1029/2005WR004715.

1. Introduction

[2] Mechanics of sediment transport is a fundamental issue in morphodynamics. When a shear turbulent flow acts on a cohesionless granular bed, sediment particles are intermittently and randomly entrained by the flow provided some convenient measure of the hydrodynamic stress acting on the bed surface exceeds a conventional threshold value. Once the sediment particles are entrained by the stream they can move as bed load or suspended load. In the case of steep gravel bed streams, bed load appears to be the dominant mode of sediment transport. In this case the mechanics of bed load is governed by the hydrodynamical interaction of the particles with the bed. When the bed is characterized by relatively high slopes, such as near the banks, along the bar fronts and in steep mountain streams, the particle velocity and the bed load transport are crucially affected by the downslope component of gravity force, both in terms of intensity and direction. Deterministic attempts to provide a theoretical description of bed load transport under uniform equilibrium conditions [*Ashida and Michiue*, 1972; *Engelund and Fredsoe*, 1976; *Wiberg and Smith*, 1985, 1989; *Sekine and Kikkaua*, 1992; *Nino and Garcia*, 1994a, 1994b] invariably consist of two main steps.

[3] In the first step an estimate of the average velocity in terms of intensity and direction of saltating particles is provided, either from a saltation model, by studying the trajectories of saltating grains over beds usually slightly inclined in the horizontal direction or, more simply, by considering an equivalent uniform translatory motion of particles.

[4] The second step is devoted to the evaluation of the average areal concentration of saltating particles, i.e., the average volume of saltating particles per unit area. Evaluation of this quantity is not an easy task because the number of particles in motion is related to the spatial and temporal frequencies and intensity of near-wall turbulent events. To overcome these difficulties many models rely on Bagnold's assumption [*Bagnold*, 1956, 1973], according to which the areal concentration of particles in motion is such that the fluid shear stress at the bed must be reduced to the critical value corresponding to the incipient motion of bed particles.

[5] The validity of Bagnold's hypothesis has been questioned since the experimental work of *Fernandez Luque and van Beek* [1976], who performed detailed observations of the dynamics of saltating particles at fairly low Shields stress and discussed the validity of Bagnold's hypothesis: for values of the latter stress smaller than about 0.1 the assumption appeared to fail.

[6] Recently, *Seminara et al.* [2002], by means of a three-dimensional generalization of Bagnold's assumption, showed that for a given particle Reynolds number and local longitudinal slope, Bagnold's assumption can only be satisfied provided the local lateral slope does not exceed a

[1]Department of Civil and Environmental Engineering, University of Florence, Florence, Italy.
[2]Now at Laboratorio Alta Versilia, Center of Research and Advanced Education for Hydrogeological Risk Prevention, Lucca, Italy.

0043-1397/07/2005WR004715$09.00

threshold value, which depends on the applied Shields stress, no matter how large the average areal concentration is. As the applied Shields stress increases, the maximum lateral inclination allowed for the occurrence of equilibrium bed load transport decreases until values of about few degrees are reached, which is well below the angle of repose. This failure motivates the abandonment of the Bagnold's constraint, even for nearly horizontal beds.

[7] On the basis of these theoretical findings, an alternative model for evaluating bed load transport on arbitrarily sloping beds has been elaborated by *Parker et al.* [2003] based on the experimental results of *Fernandez Luque and van Beek* [1976]. According to this model the fluid shear stress at the bed drops to the critical value for particle motion only when there is no motion (static equilibrium); on the contrary, when bed load transport occurs, shear stress at the bed must be above the critical value in order for the flow to entrain grains. Equilibrium is then achieved through a balance between an entrained sediment flux and a deposited flux (dynamic equilibrium). Applications of this model on a bed with finite slope in an arbitrary direction show that the intensity of bed load transport increases with the external applied shear stress faster than on horizontal beds, and more so as the longitudinal and lateral slopes increase. Moreover, a comparison with the results obtained in the case of linearized formulations devised for beds that are modestly sloping suggests that the classical approaches of bed load transport as a function of local slope can lead to great underestimations.

[8] In the present work, the effect of gravity on bed load transport due to water flow has been investigated by means of an experimental activity being the main objective to provide experimental support to the theoretical findings of *Seminara et al.* [2002] and *Parker et al.* [2003]. The paper proceeds as follows: After a brief summary of the *Parker et al.* [2003] model (section 2), the experimental apparatus, which consists of a laboratory flume equipped with an image acquisition system, is presented and discussed (section 3). Measurements were taken employing different techniques on the basis of volumetric sampling, laser Doppler anemometry, and image acquisition and processing (sections 3.1 and 3.2). The results of the experimental observations of the bed load transport mechanisms over a nonerodible arbitrarily sloping bed at low Shields stress are shown in section 4 and compared to the computed values from the *Parker et al.* [2003] model in terms of the average properties of collective motion of sediment particles for various hydraulic conditions and longitudinal and transversal inclinations of the bed. The experimental findings are discussed with regard to the results from the linear approximation of the *Parker et al.* [2003] model and to some aspects related to bed load transport on erodible beds in section 5. Finally, conclusions are drawn in section 6.

2. Theoretical Framework of the *Parker et al.* [2003] Model

[9] The main physical aspects and equations of the *Parker et al.* [2003] model are reported here, while the reader is referred to the latter paper for details of the analysis. The bed load transport vector per unit width, which is made dimensionless with the Einstein's scale, is evaluated as follows:

$$\hat{\mathbf{q}} = \hat{\xi} \cdot \hat{\mathbf{V}}_p \tag{1}$$

where $\hat{\xi}$ is the volume areal concentration of bed load made dimensionless with the sediment diameter D and $\hat{\mathbf{V}}_p$ is the layer-averaged mean velocity vector of bed load particles made dimensionless with $\sqrt{(s-1)gD}$, where g is gravity and s is the relative sediment density.

[10] The average particle velocity vector in terms of intensity $|\hat{\mathbf{V}}_p|$ and direction $\hat{\mathbf{s}}_p$ is obtained by imposing a vectorial balance between averaged active and resistive forces, where the former is represented by the drag force $\mathbf{F}_D$ and the tangential component along the bed of the submerged particle weight; the latter interprets the effect of continuous or intermittent hydrodynamic interactions of particles with the bed and is estimated through a coefficient of dynamic friction μ_d. This balance is written as follows:

$$\mathbf{F}_D + \rho g(s-1)V\mathbf{k}_t = \mu_d \rho g(s-1)V|\mathbf{k}_n|\hat{\mathbf{s}}_p \tag{2}$$

where ρ is the water density, V is the particle volume, $\mathbf{k}_n$ and $\mathbf{k}_t$ are the projections of the unit vertical vector in the normal and tangential direction to the bed, respectively. Here the drag force is a vector aligned with the relative fluid particle velocity, which reads:

$$\mathbf{F}_D = \frac{1}{2}\rho C_d \frac{\pi D^2}{4}\left(\mathbf{U} - \mathbf{V}_p\right)\left|\mathbf{U} - \mathbf{V}_p\right| \tag{3}$$

where C_d is the drag coefficient of the particle, $\mathbf{V}_p$ is the dimensional particle velocity vector, $\mathbf{U}$ is the vector of the mean tangential fluid velocity in the bed load layer with direction $\hat{\mathbf{s}}$ and intensity $u_* \cdot f$, with u_* being the friction velocity and f coming from the logarithmic velocity distribution law of the wall. Equation (2) using the definition (3) in dimensionless form reads:

$$\left|\sqrt{\tau_*}\hat{\mathbf{s}} - \frac{|\hat{\mathbf{V}}_p|}{f}\hat{\mathbf{s}}_p\right|\left(\sqrt{\tau_*}\hat{\mathbf{s}} - \frac{|\hat{\mathbf{V}}_p|}{f}\hat{\mathbf{s}}_p\right) = \lambda^2\tau_{*co}\left(|\mathbf{k}_n|\hat{\mathbf{s}}_p - \frac{\mathbf{k}_t}{\mu_d}\right) \tag{4}$$

where τ_* is the dimensionless Shields stress based on the fluid boundary shear stress $\boldsymbol{\tau}_{fB}$ that would occur at the bed in the absence of a moving bed load layer; λ is a dimensionless coefficient that is a function of the ratio between the critical Shields stress for the cessation of the bed load motion and the critical Shields stress τ_{*co} on a horizontal bed for the onset of sediment motion. Note that in general the direction of particle motion $\hat{\mathbf{s}}_p$ does not coincide with the direction of the applied shear stress $\hat{\mathbf{s}}$ unless the bed is longitudinally tilted only; the angle between the two latter vectors is named deviation angle and denoted by ψ. In particular, the theoretical results of *Seminara et al.* [2002] suggest that for a given bed inclination, ψ decreases as the Shields stress increases.

[11] In order to find the average areal concentration of sediment in motion, a dynamic equilibrium of a volume of fluid sediment mixture adjacent to the unit area of the bed,

with height equal to the characteristic thickness of the saltation layer, is imposed. This balance reads:

$$\boldsymbol{\tau}_{fB} + \rho g(s-1)\hat{\xi} D \mathbf{k}_t = \boldsymbol{\tau}_{fb} + \boldsymbol{\tau}_{sb} \tag{5}$$

that is, the fluid shear stress $\boldsymbol{\tau}_{fB}$ and the contribution of the particle weight in the direction tangential to the bed are given by the actual fluid shear stress at the bed $\boldsymbol{\tau}_{fb}$ in the presence of a bed load layer and the shear stress due to the solid phase $\boldsymbol{\tau}_{sb}$, which is realized by means of momentum transfer through oblique particle collisions with the bed. The general expression of the shear stress due to momentum transferred to the saltating particle is the following:

$$\boldsymbol{\tau}_{sb} = \mu_d \rho g(s-1)\hat{\xi} D |\mathbf{k}_n| \hat{\mathbf{s}}_p \tag{6}$$

Equations (5) and (6) can be rearranged in the following form:

$$\boldsymbol{\tau}_{fb} = \boldsymbol{\tau}_{fB} - \boldsymbol{\tau}_D \tag{7}$$

where $\boldsymbol{\tau}_D$ is the drag stress due to the transfer of momentum per unit volume per unit time from the fluid phase to the solid phase evaluated as follows:

$$\boldsymbol{\tau}_D = \frac{\mathbf{F}_D}{V}\, \hat{\xi} D \tag{8}$$

The exact generalization of Bagnold's hypothesis then poses the following constraint:

$$\left|\boldsymbol{\tau}_{fb}\right| = \tau_{fc} \tag{9}$$

where τ_{fc} is the critical shear stress for sediment motion for a given longitudinal and transversal inclination of the bed. A simple physical explanation for the existence of the threshold value of the lateral bed inclination above which equation (9) has no solution is related to the vectorial nature of Bagnold's hypothesis. In fact, in the case of a bed longitudinally tilted only, the average motion is unidirectional and particle drag is aligned with the incident average fluid motion. In this case the fluid shear stress at the bed can always be reduced to the critical value by appropriately increasing the resultant drag force, i.e., the concentration of saltating particles. This is not the case when the bed is arbitrarily sloping as particle drag is no longer aligned with the fluid shear stress; in these conditions it can be shown that $\boldsymbol{\tau}_{fb}$ exhibits a minimum with the areal concentration. Therefore it follows that whenever such a minimum exceeds the critical value of the shear stress appropriate for the longitudinal and lateral slopes of the bed, then the Bagnold's constraint cannot be satisfied. In other words, at low Shields stress Bagnold's assumption is unduly severe. When the bed is locally tilted with relatively high slopes, gravity contributes more to particle motion and therefore causing the solid phase to drain less momentum from the liquid phase.

[12] The Bagnold constraint is replaced with an entrainment formulation, according to which a dynamic equilibrium is maintained by a balance between entrainment of bed grains into the bed load layer and deposition of bed load grains onto the bed. The dimensionless entrainment flux of bed particles into the bed load layer $\hat{E}$ is determined with an empirical function that ultimately agrees with the experimental results of *Fernandez Luque and van Beek* [1976]. In particular it can be expressed as an increasing function of the excess of the fluid shear stress at the bed over the critical shear stress for the onset of particle motion and has the following expression:

$$\hat{E} = A_e \cdot \left(\tau_{*b} - \tau_{*c}\right)^{3/2} \tag{10}$$

where A_e is a parameter to be evaluated, τ_{*b} is the dimensionless Shield stress based on $\boldsymbol{\tau}_{fb}$ and τ_{*c} is the critical Shields stress on an arbitrarily sloping bed. Note that the entrainment flux vanishes when $\tau_{*b} = \tau_{*co}$ and is a nonnegative, monotonically increasing function of $\tau_{*b} - \tau_{*c}$, which may be taken as a measure of the residual turbulent activity at the bed which appears to be responsible for the sediment motion. Equilibrium bed load transport conditions are therefore reached not when the fluid shear stress at the bed reaches the threshold value, but when the entrainment rate of bed particles into the bed load layer equals the deposition rate of bed load particles onto the bed. The dimensionless deposition rate $\hat{D}$ is modeled with the following:

$$\hat{D} = A_d \cdot \left(\tau_* - \tau_{*b}\right)^{1/2} \hat{\xi} \tag{11}$$

where A_d is a parameter to be evaluated. Therefore, when combining equations (10) and (11) at equilibrium condition, the following equation for the dimensionless sediment concentration is found:

$$\hat{\xi} = \frac{A_e}{A_d} \frac{\left(\tau_{*b} - \tau_{*c}\right)^{3/2}}{\left(\tau_* - \tau_{*b}\right)^{1/2}} \tag{12}$$

Equation (12) shows that the average areal concentration of particles increases quasi-linearly with the excess of residual Shields stress, a result that is strongly suggestive of the fact that the latter quantity may indeed be taken as a measure of the entrainment capacity of the stream. Equation (5) written in a dimensionless form and employing equation (12) reads:

$$\tau_{*b} = \left| \tau_* \hat{\mathbf{s}} - \mu_d \frac{A_e}{A_d} \frac{\left(\tau_{*b} - \tau_{*c}\right)^{3/2}}{\left(\tau_* - \tau_{*b}\right)^{1/2}} \cdot \left(|\mathbf{k}_n| \hat{\mathbf{s}}_p - \frac{\mathbf{k}_t}{\mu_d} \right) \right| \tag{13}$$

The model requires as input various parameters, namely C_d, f, A_e, A_d, λ, the dynamic friction coefficient on a horizontal bed μ_{do}, the ratio of the lift and drag coefficients C_l/C_d, and the angle of repose of the sediments. The general method used to obtain a solution is as follows: equation (4) is solved iteratively for $|\hat{\mathbf{V}}_p|$ and $\hat{\mathbf{s}}_p$; equation (13) is then solved iteratively for τ_{*b} with $\hat{\xi}$ calculated from equation (12). Substituting the solution for $|\hat{\mathbf{V}}_p|$, $\hat{\mathbf{s}}_p$ and $\hat{\xi}$ into equation (1), the dimensionless bed load transport rate vector per unit width $\hat{\mathbf{q}}$ is found.

3. Experimental Setup and Activity

3.1. Experimental Apparatus

[13] The motion of saltating bed load particles was investigated in a free surface laboratory flume. The experiments were carried out in a tilting, recirculating flume, 10 m

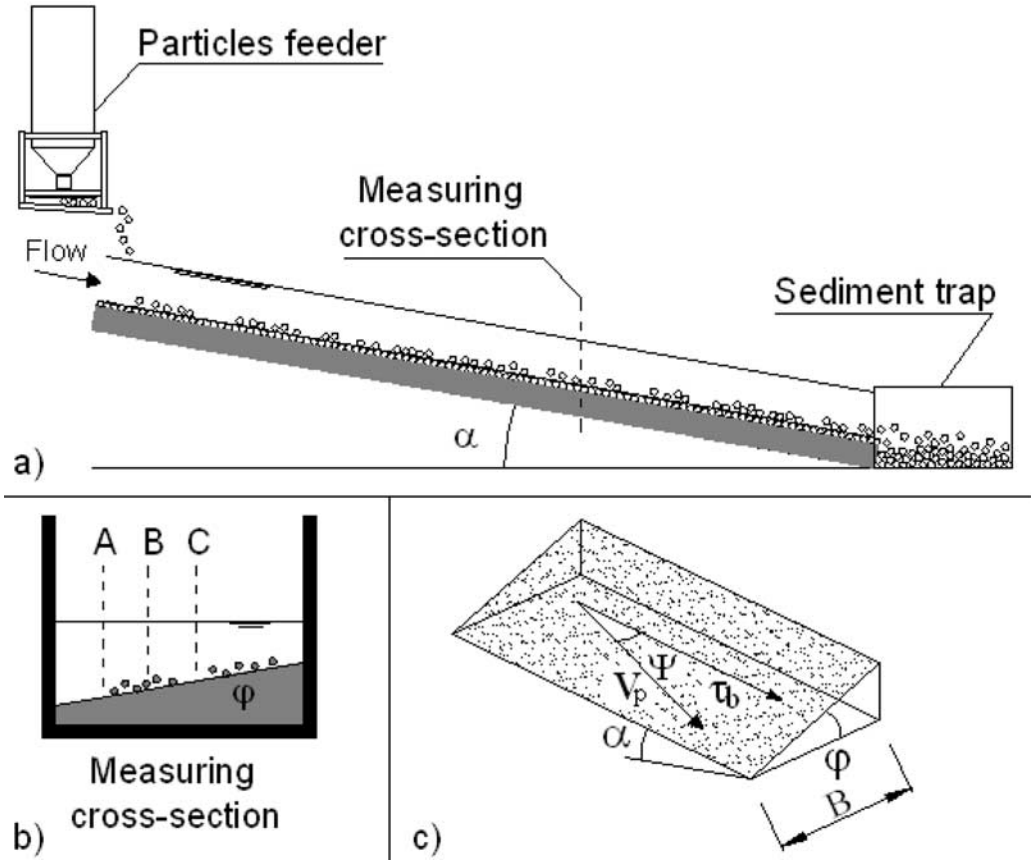

Figure 1. Sketch of the experimental apparatus. (a) Lateral view of the nonerodible bed. (b) Measuring cross section where A, B, and C are the locations where the vertical profiles of flow and particle velocity were acquired. (c) Notation: in the case of a bed with a transversal inclination φ, the average particle velocity V_p deviates from the direction of the bed shear stress τ_b at an angle ψ.

long, 0.365 m wide and 0.45 m deep, equipped for clear water flows up to 28 L/s and slope adjustment up to 5°. In order to obtain higher bed inclinations, a 1.5 m long 0.23 m wide nonerodible plane bed was built inside the downstream part of the flume with inclination adjustable up to 15° (Figure 1). The plane bed was artificially roughened with the same particles fed into the flume. Water flow was supplied at one end of the flume from a centrifugal pump and the water discharge was monitored by an electromagnetic flowmeter. The sediment particles were fed at a constant discharge by means of a travolator type sediment feeder positioned above the upstream part of the plane bed: sediments entered the flume at the beginning of the plane bed and were collected at the end of the plane bed by the sediment trap. Measurements were taken in a cross section located in the downstream part of the plane bed.

[14] The sediment particles were represented by steel particles with a density of 7850 kg/m^3, shaped like disks with almost uniform size diameters of 3 mm and thicknesses of 0.6 mm. The equivalent particle sieve diameter D is 2.6 mm. The reason for using these disk-shaped steel particles was related to the extreme difficulties in finding suitable sediments for the present experiments. In fact the sediments had to be movable in a wide range of flow conditions and bed inclinations with the ratio of water depth to particle size sufficiently high to allow particle saltation.

[15] A schematic representation of the experimental setup is shown in Figure 2. A monocomponent laser Doppler anemometer placed perpendicular to the glass wall was employed to measure both sediment particle velocity and flow velocity distribution along the three verticals in the measuring cross section (see Figure 1b). The particle velocity field was also studied through a digital image analysis of particle motion in order to measure the intensity and direction of the averaged velocity vectors. A computer controlled the digital camera and the illumination system for the acquisition of particle images through a timing control device; video images of bed load particles saltating over the bed were taken from the upper side of the flume and acquired by the frame grabber.

[16] In the case of a longitudinal and transversal sloping bed, different values of the bed shear stress along the cross section induced different local sediment transport equilibrium conditions. A sediment trap (Figure 3) positioned at the downstream end of the plane bed was employed to quantify the sediment transport discharge: the sediment trap was divided into 5 zones in order to measure different values of the sediment transport rate along the cross section. The collected sediments were then dried and weighted.

3.2. Image Processing System

[17] The measurements of fluid velocity using digital image processing can be classified into two categories

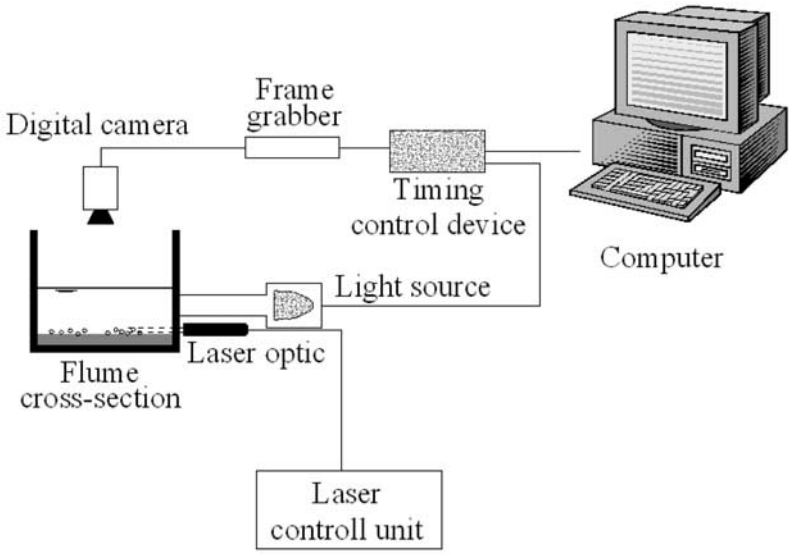

Figure 2. Sketch of the experimental setup.

[*Adrian*, 1991], PIV (particle image velocimetry) and PTV (particle tracking velocimetry), depending on how the displacement vectors are extracted from particle images. These techniques have been applied to study velocity fields of fluids and recently to investigate the bed load movement of sediment particles in a laboratory flume [*Hu and Hui*, 1996; *Nino and Garcia*, 1998; *Papanicolaou et al.*, 1999; *Lee et al.*, 2000]. In both techniques, the flow is seeded with small tracer particles and then illuminated by a series of laser pulses at a known time interval. The scattered light from the seeding particles in the illuminated plane is recorded as a particle image by a device such as a CCD (charge-coupled device). The PIV evaluates flow field velocity from digital analysis of a pair of images. The PTV tracks individual particle in consecutive image frames and evaluates the directionally resolved displacement vector for each matched particle pair. The image based technique employed here is a particle tracking approach applied to a single pair of images with a short interframing time (as in PIV analysis) instead of tracking the same particle in a series of images with a constant time interval (as in PTV analysis). Then, the short interframing time and the limited number of particles in motion allow one to track sediment particles from image A to image B of a pair in a given time interval and evaluate the velocity vector.

[18] In the present experiments, measurements of particle motion were obtained through an image analysis technique that was based on the following components: seeding, illumination, image recording and image processing.

[19] The seeding was based on particle tracers lightened by pulsating light and made visible using a digital camera: a collimated light source located on a side of the flume illuminated the bed load layer, while not interfering with the free water surface. In the experiments, the steel sediment particles acted as tracers and their velocity was then measured. In fact, steel material was highly reflective and visible on the camera, while the fixed bed was dyed black to more easily observe particle motion.

[20] The illumination system consists of a stroboscopic pulsating light which was able to produce short bursts of lamp light to acquire pairs of images. The frequency range of coupled images was 0.5–5 Hz with a resolution of 0.1 Hz, while the interframing time between two images of a single couple was in the range 1–10 ms with a resolution of 0.1 ms. The time interval between each couple led us to consider image couples as independent measurements. The digital camera for the image recording was characterized by a high resolution (max resolution 1360 × 1024 pixel), which allowed images where a single particle consisted of a bulk of pixels, and a short interframing rate. This led two images to be captured in which particle tracers covered a relative small distance into the bed plane. The interrogation area had a longitudinal length of about 16 cm and a width of 22 cm. Both the digital camera and the system illumination were controlled and synchronized by a computer. The CCD plane was oriented parallel to the

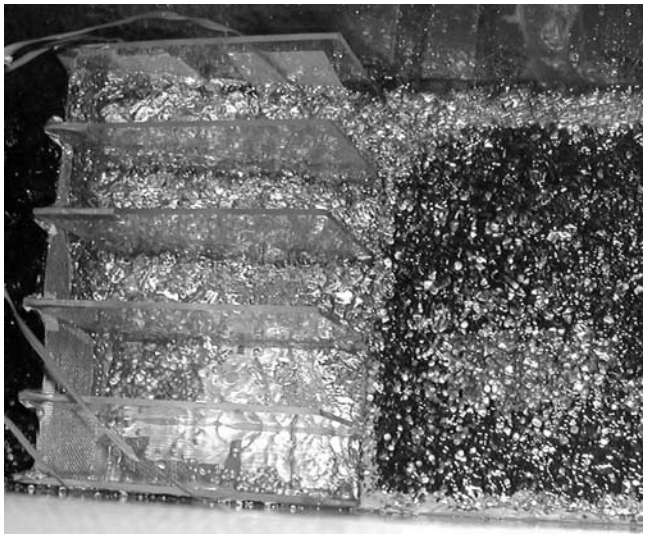

Figure 3. View of the sediment trap to measure bed load transport discharge, at the end of an experiment. Particle deposit on a side is due to the bed shear stress under the critical conditions for the onset of sediment motion.

Table 1. Main Experimental Conditions: Longitudinal Bed Inclination α, Transversal Bed Inclination φ, Flow Discharge Q, and Sediment Feeding Rate Q_s

α, deg	φ, deg	(Q,Q_s), L/s, g/s
1.72	0	(11.8,19.5) (13.56,29.4) (15.6,61.75) (18,80.7)
5	0	(2.68,11.1) (3.1,28) (3.56,57) (3.95,72) (5.02,122) (7,159) (9,215)
10	0	(1.61,63) (2.15,122) (2.61,177) (3.1,167) (3.61,214) (4.14,228) (4.6,290) (5.1,322) (5.6,282) (6.1,349) (7.01,403)
15	0	(0.8,33) (1.1,69) (1.4,122) (1.9,221) (2.4,213) (3,306) (3.5,295)
1.72	10	(12.02,28) (15.4,48)
1.72	20	(12.3,44) (15.8,57)
5	5	(2.68,57) (3.1,69) (4.06,105) (4.98,122) (5.98,165) (7.49,182)
5	10	(2.68,75) (4.07,111) (5.5,155) (7.02,187)
5	15	(3.67,89) (5.05,111) (6.1,133) (7.5,151)
5	20	(4.43,151) (5.95,167) (7.15,198) (8.5,241)
10	5	(1.4,72) (2.1,100) (3,151.5) (4.5,174)
10	10	(1.5,89) (2.35,111) (3.11,136) (4.5,198)
10	15	(2.53,122) (3.53,155) (4.5,213)
10	20	(1.5,111) (2.5,138) (3.5,190) (4.5,241)
15	5	(1.4,120) (2.13,180) (3.0,322)
15	10	(1.5,122) (2.35,198) (3.11,295)
15	15	(2.16,151) (2.5,161) (3.0,232)
15	20	(2,159) (2.53,185) (3.0,228)

sloping bed layer. The measured particle velocity field was the one projected on a plane parallel to the bed and hence corresponding to the local mean value of the solid phase saltating and rolling on the sloping bed.

3.3. Experimental Activity

[21] The experimental activity was focused on the investigation of the bed load transport mechanism when transversal and longitudinal slopes are not negligible and low values of the applied Shields stress occur. The experiments consist of two sets of data: (1) experiments on a plane bed with no transversal slope and (2) experiments on a laterally tilted plane bed. The longitudinal inclination α was 1.72°, 5°, 10°, 15°, while the transversal inclination φ was 5°, 10°, 15°, 20°, combined together (see Figure 1 for notation). For all combinations of sloping bed and different values of the flow discharge Q, bed load transport rate at equilibrium conditions along the cross section and particle and flow velocity profiles with laser Doppler were determined. For some of the experimental flow conditions, experiments using the image analysis technique were performed in order to compare independent sets of data regarding particle velocity and to obtain an estimation of the velocity deviation angle. The main experimental conditions are reported in Table 1, where for each set of bed inclinations, the flow discharge Q and the sediment feeding rate Q_s are shown. A total of 78 experiments were carried out, 29 of them with longitudinal inclination only. Each experiment lasted several hours.

[22] The experiments were carried out according to the following procedure. First the local sloping nonerodible bed was adjusted to the given values of longitudinal and transversal inclinations. The flow was then started in the flume and steady condition was reached. With regards to the liquid phase, measurements of flow discharge and velocity were carried out by means of an electromagnetic flowmeter and a laser Doppler anemometer. In particular, along the measuring cross section (Figure 1b), three vertical velocity profiles were defined through at least 10 points along the flow depth and located at a distance of 5, 9 and 13 cm from the right side of the flume, that is from deeper to shallower water depth. With regards to the solid phase, the feeding of sediments into the channel was established to match the sediment transport capacity in equilibrium with the given flow discharge. The bed load transport discharge was measured with the sediment trap. The profiles of particle velocity within the saltation layer were measured with the laser Doppler anemometer in the same locations as the flow velocity profiles, and a layer-averaged value was evaluated. Finally, the measurements using the image analysis technique were conducted: an image of a squared grid was preliminarily acquired to obtain the calibration coefficients in the vertical and horizontal directions, and then several sequences of image couples were acquired in order to collect a representative set of data.

4. Results

[23] Preliminary experiments were carried out in order to check the behavior of the experimental setup and to define basic parameters such as equivalent roughness of the nonerodible plane bed and critical Shields stress for the onset of sediment motion. The equivalent roughness of the nonerodible plane bed was evaluated for the condition of fully turbulent flow and appeared to range around $0.8-1.2$ times the particle diameter. The critical Shields stress τ_{*co} for the onset of sediment motion in the case of vanishing bed slopes was experimentally estimated to be about 0.03. Tests on the sediment mobility in the case of a streamwise finite slope showed a reasonable agreement with the critical value of the Shields stress, that was corrected to take into account the effect of the streamwise slope.

[24] The Shields stress was evaluated along the measuring cross section by means of the measured averaged velocity profiles: the friction velocity u_* and the bed roughness length were estimated via regression analysis fitting a logarithmic velocity profile in the near bed region in agreement with the trend showed by the data, and hence the bed shear stress was evaluated through the latter parameters. Measured data showed decreasing values of the applied Shields stress with the reduction of the water depth along the cross section due to lateral inclination. In Figure 4 the ratio of the applied Shields stress to the critical Shields stress for the incipient particle motion on horizontal beds τ_*/τ_{*co} is plotted as a function of the distance d from the side with higher water depth, which was made dimensionless using the channel width B, for different values of flow discharge. This Shields stress trend is confirmed by the presence of a depositional area that was observed during the few lowest flow discharge experiments in the shallower part of the cross section where Shields stress attained values under the critical value for the onset of sediment motion.

[25] In the following, mean values of sediment velocity, bed load transport rate and areal concentration are presented and compared with the theoretical results predicted by *Parker et al.* [2003] and the experimental findings of other authors; a goodness of fit test between observed and calculated values is then presented.

[26] The predicted values of the particle velocity intensity $|\hat{\mathbf{V}}_p|$ and the deviation angles ψ are obtained from

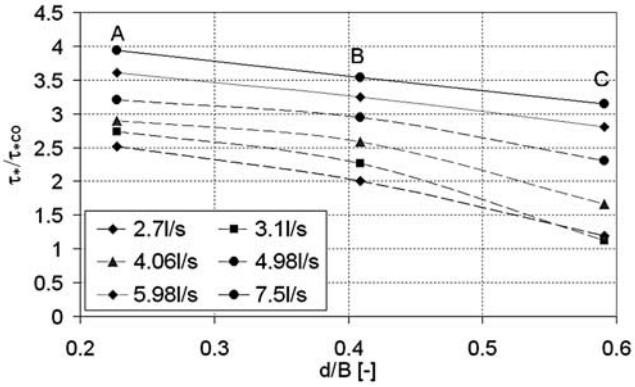

Figure 4. Shields stress ratio τ_*/τ_{*co} versus dimensionless transversal distance along the cross section for different flow discharges and in the case of a bed inclination $\alpha = 5°$, $\varphi = 5°$. A, B, and C are the verticals of measurements.

equation (4), while the Shields stress at the bed τ_{*b} is evaluated with equation (13) and the dimensionless areal concentration $\hat{\xi}$ with equation (12). The theoretical quantities are obtained in the case of the following values of the main parameters: drag coefficient $C_d = 0.4$, ratio between lift and drag coefficient $C_l/C_d = 1.25$, dynamic friction coefficient in the case of a horizontal bed $\mu_{do} = 0.3$, angle of repose $\phi = 35°$, and the same values as adopted by *Parker et al.* [2003] are given to the remaining parameters.

4.1. Particle Velocity

[27] Particle velocity data were acquired with the above described techniques: laser Doppler anemometer allows knowledge of the longitudinal component of the averaged particle velocity within the saltation layer, and the image analysis techniques revealed the intensity and angle deviation of the velocity vector. The layer-averaged particle velocity profile obtained with laser Doppler anemometer was related to the local value of the Shields stress estimated in the same vertical of measurements along the cross section.

[28] The image processing analysis of a single pair of images is divided into two steps. The first step is to locate all objects of interest in each frame, determine each object's position (center of mass), and store that information. The second step is to determine which of these objects can be unambiguously identified in successive frames and assign unique numerical labels to each distinguishable object.

[29] The used approach requires that the distance an object moves (from frame to frame) be smaller than the typical distance between objects and that there are few particles in motion (about less then 100). In this way particle centroid positions can be easily identified in each frame and the ambiguousness related to the tracked direction is reduced.

[30] The experimental conditions for the particle tracking experiments were chosen among the whole set of acquired data in order to satisfy the following requirements and to guarantee the best image quality: the main requirements were that the entire cross section was invaded by the flow and no air bubbles were associated with the oscillations of the water free surface reflecting the light. Along the cross section, only the values of bed shear stress and particle velocity corresponding to reasonable values of water depth of at least 3–4 times the particle size were selected.

[31] According to these criteria, the experiments carried out in the case of the highest longitudinal inclination (15°) were characterized by concentrations of particles in motion too high to be analyzed with the present image technique, while in the case of the highest transversal inclinations (15°, 20°) the particle motion took place in a narrow portion of the cross section with extremely variable water depth along the cross section and hence strong nonhomogeneous illumination.

[32] In order to apply the present image technique to the selected experiments, some criteria needed to be set. First, all the objects that have a smaller area than diameter size in equivalent pixels were eliminated: in this way the background noise was avoided, as in general the effective particles were much bigger than the noise particle due to light reflection. Second, the maximum distance an object can move from frame to frame needed to be set. In the area specified by this distance cutoff radius only one object was unambiguously tracked; that is why the approach required few particles in motion. An example of a single pair of images is shown in Figure 5. Numbered labels indicate particle displacements in each frame. The particles located in the noisy areas of the image, i.e., near the glass wall or where no motion occurred, were not counted in the analysis. The conversion factors from pixels to millimeters were

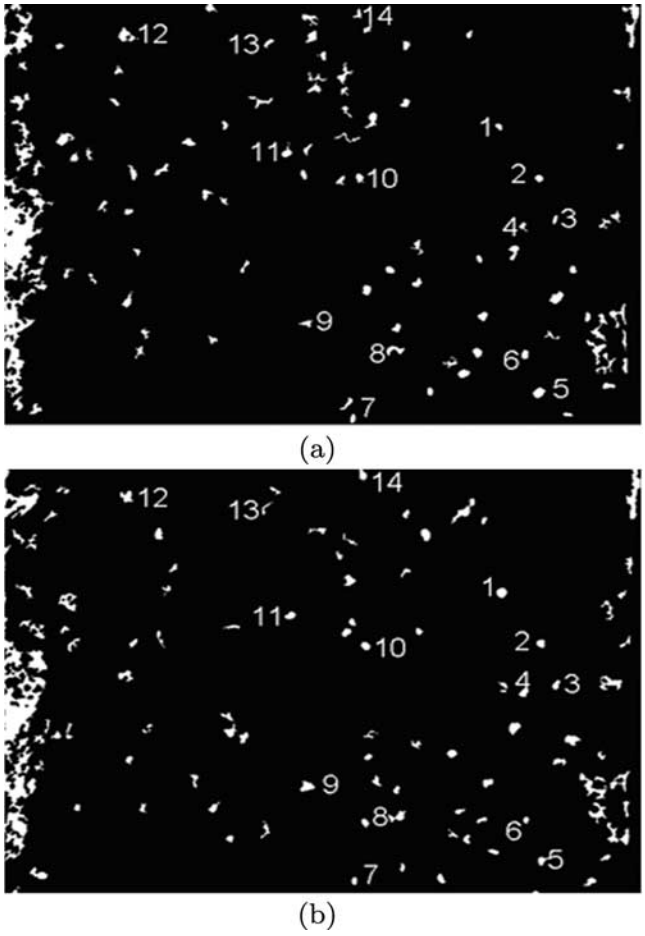

Figure 5. (a and b) Pair of analyzed images ($\alpha = 5°$, $\varphi = 10°$, $Q = 7.02$ L/s). Labels indicate a sample of tracked objects.

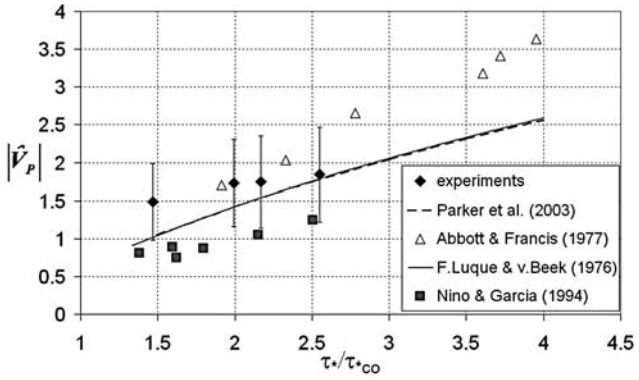

Figure 6. Comparison between the experimental values of dimensionless particle velocity intensity and findings from other authors, in the case of $\alpha = 1.72°$ and $\varphi = 0°$.

evaluated from the calibration image of the squared grid laid on the bed acquired at the beginning of the activity.

[33] The postprocessing data was focused on removing outliers in order to improve the quality of the data; several criteria were used: particles move according to the flow direction, particles cannot move against gravity even if they can be carried by the flow for small distances, particles that do not move or that oscillate around their positions were removed from the averaging. Finally, the last step was the evaluation of particle velocity from the tracked locations and the interframing time between images, and the averaging of velocity vectors according to their position. To this aim the bed surface was divided into six stripes: the velocity vectors were averaged along each stripe, and the bed shear stress was evaluated from the corresponding measured bed shear stress profile.

[34] The dimensionless mean value of particle velocity intensity as a function of the ratio τ_*/τ_{*co} is reported in Figure 6 in the case of a longitudinal bed inclination of 1.7° The experimental data seems to confirm the theoretical findings of the model proposed by *Parker et al.* [2003] and are in reasonable agreement with the experimental findings of *Nino and Garcia* [1994a] and *Abbott and Francis* [1977] and the experimental interpretation by *Fernandez Luque and van Beek* [1976], at least in the range of the investigated values of τ_*/τ_{*co}. The relatively high values of the particle velocity observed by *Abbott and Francis* [1977] refer to the motion of single grains in a water stream and can differ from the results obtained in the case of a populated layer of moving grains.

[35] The dimensionless longitudinal component of the averaged particle velocity is plotted as a function of the Shields stress ratio τ_*/τ_{*co}. In Figure 7 the comparison between the experimental observations and the theoretical model for each configuration of the sloping bed and flow

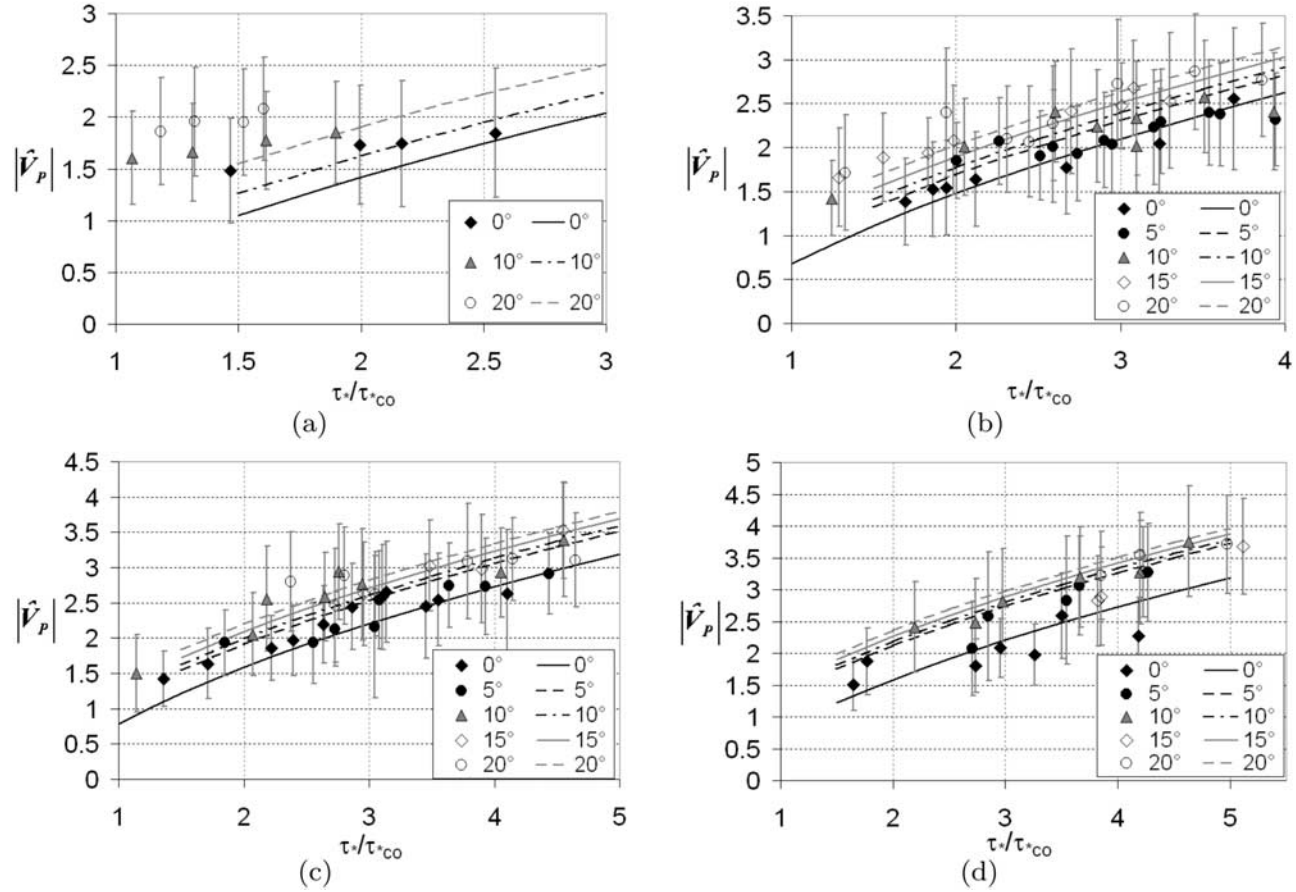

Figure 7. Dimensionless particle velocity intensity: experimental data (points) compared to the theoretical model of *Parker et al.* [2003] (lines) for different bed inclinations: (a) $\alpha = 1.72°$ and $\varphi = 0°$, 10°, and 20°; (b) $\alpha = 5°$ and $\varphi = 0°$, 5°, 10°, 15°, and 20°; (c) $\alpha = 10°$ and $\varphi = 0°$, 5°, 10°, 15°, and 20°; and (d) $\alpha = 15°$, $\varphi = 0°$, 5°, 10°, 15°, and 20°.

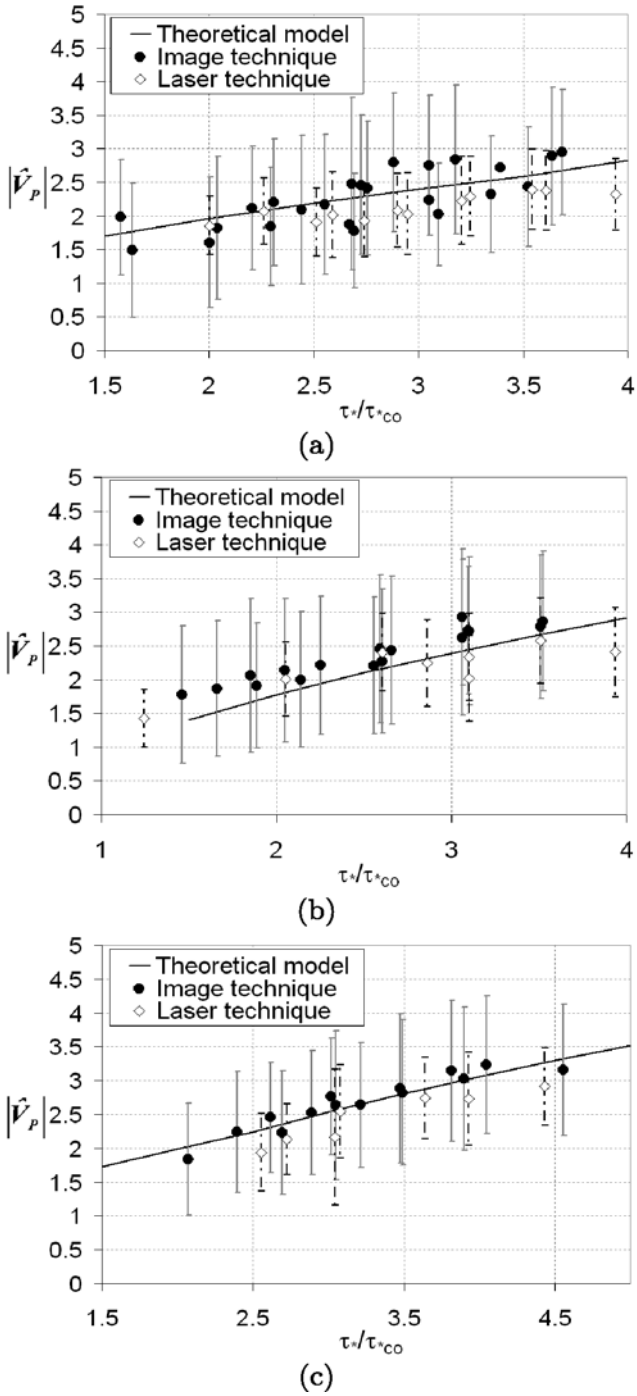

Figure 8. Comparison between the experimental values of the dimensionless particle velocity intensity with image and laser techniques (points) and the theoretical model (line) of *Parker et al.* [2003]: (a) $\alpha = 5°$, $\varphi = 5°$, (b) $\alpha = 5°$, $\varphi = 10°$, and (c) $\alpha = 10°$, $\varphi = 5°$.

conditions is shown: Figures 7a–7d show different sets of data with the same longitudinal inclination and different values of the transversal inclination; dots indicate the mean experimental data, the vertical lines indicate the root mean squares, and the curves indicate the theoretical model. The dimensionless particle velocity is seen to increase with the applied Shields stress and with higher values of the transversal bed inclination for the same value of α. Experimental values show good agreement with the theoretical model proposed by *Parker et al.* [2003].

[36] Because of the fact that the contribution of the transversal component of the particle velocity is much smaller than the total intensity, it seems reasonable to compare the longitudinal component of particle velocity from the laser technique and the total intensity of particle velocity from the image analysis technique as independent sets of data (Figure 8) in order to test the agreement of

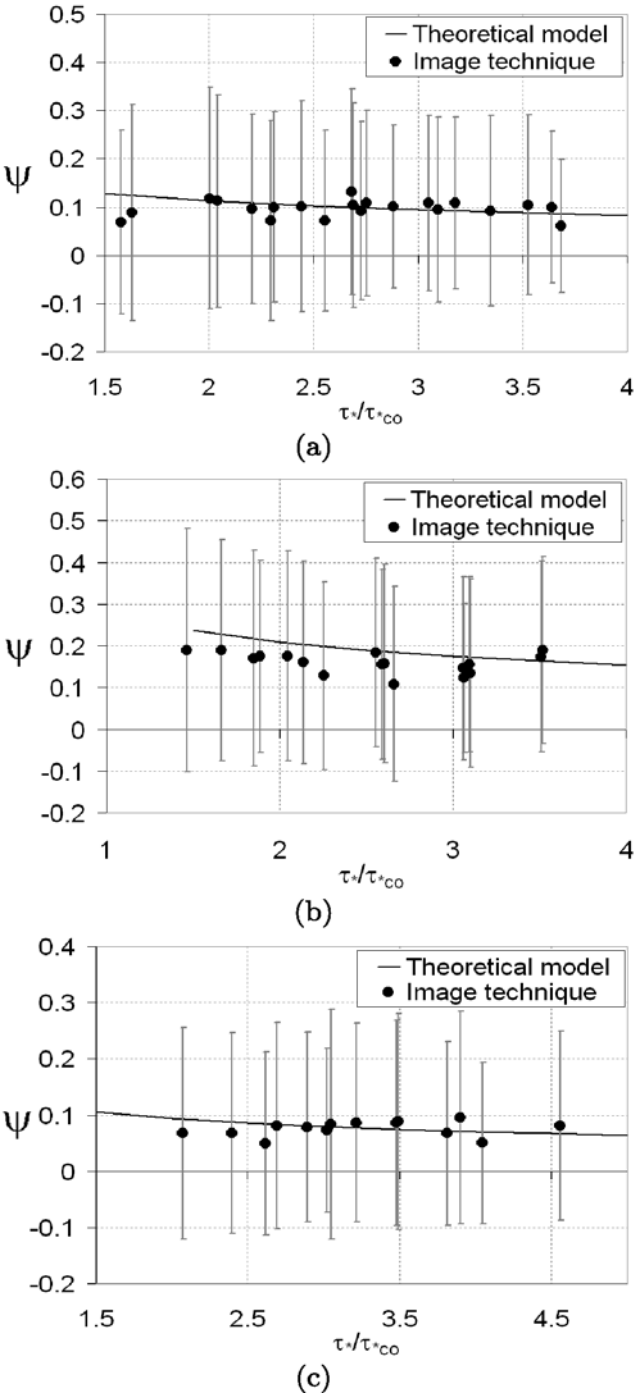

Figure 9. Comparison between the experimental particle deviation angle (points) and the theoretical model (line) of *Parker et al.* [2003]: (a) $\alpha = 5°$, $\varphi = 5°$, (b) $\alpha = 5°$, $\varphi = 10°$, and (c) $\alpha = 10°$, $\varphi = 5°$.

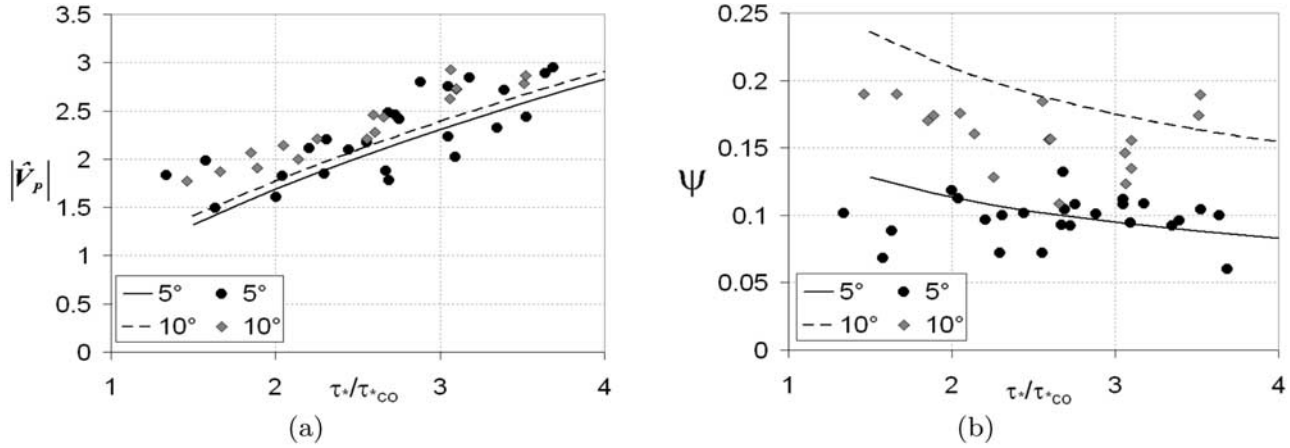

Figure 10. Effect of the transversal inclination on particle velocity: Comparison between the experimental data obtained by the image technique (points) and the theoretical model (lines) of *Parker et al.* [2003], in the case of longitudinal inclination $\alpha = 5°$. (a) Dimensionless particle velocity intensity: $\varphi = 5°$ and 10°. (b) Particle deviation angle: $\varphi = 5°$ and 10°.

experimental measurements: the trend of the data is shown to be the same; also the root mean squares of the data are of the same order of magnitude for both techniques. This latter finding suggests the capability of the present image technique to adequately describe the particle velocity in terms of intensity and direction.

[37] Particle deviation angles estimated from image analysis are shown in Figure 9 where deviation angle is plotted against the Shields stress ratio for three conditions of the sloping bed. The deviation angle is largely dependent on the value of transversal inclination and lightly dependent on the Shields stress; it is expected to slightly decrease with higher values of the applied Shields stress and to increase with higher values of the transversal inclination. The relatively high values of the error bars in Figure 9 are mainly due to the intrinsic mechanism of the saltating particles on an artificially roughened bed.

[38] Finally, it is worth pointing out the effect of the longitudinal and transversal inclinations on the particle deviation angle. In Figure 10, different sets of data with the same longitudinal inclination $\alpha = 5°$ and different transversal inclinations $\varphi = 5°$, 10° are compared: the velocity intensity appears to slightly increase as the transversal inclination increases; the particle deviation angle has much higher values for higher values of the transversal inclination. In Figure 11, different sets of data with the same transversal inclination $\varphi = 5°$ and different longitudinal inclinations $\alpha = 5°$, 10° are compared: the velocity intensity increases with increasing values of the longitudinal inclination, while the particle deviation angle decreases.

4.2. Sediment Transport Rate

[39] The bed load sediment transport discharge was measured while the sediment transport capacity was in dynamic equilibrium with the given flow condition. The input solid discharge was fed to match the maximum transport rate, but, due to the transversal inclination of the bed, local values of the bed load transport rate differed along the cross section. The sediment trap allowed measurements of the local values of bed load transport intensity, and the 5 zones of the sediment trap were related to different

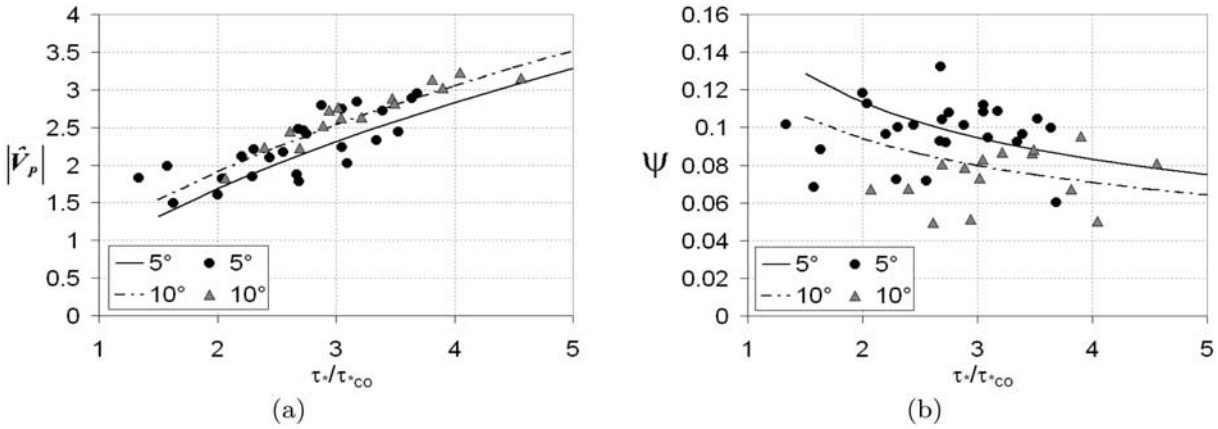

Figure 11. Effect of the longitudinal inclination on particle velocity: Comparison between the experimental data obtained by the image technique (points) and the theoretical model (lines) of *Parker et al.* [2003], in the case of transversal inclination $\varphi = 5°$. (a) Intensity: $\alpha = 5°$ and 10°. (b) Deviation angle: $\alpha = 5°$ and 10°.

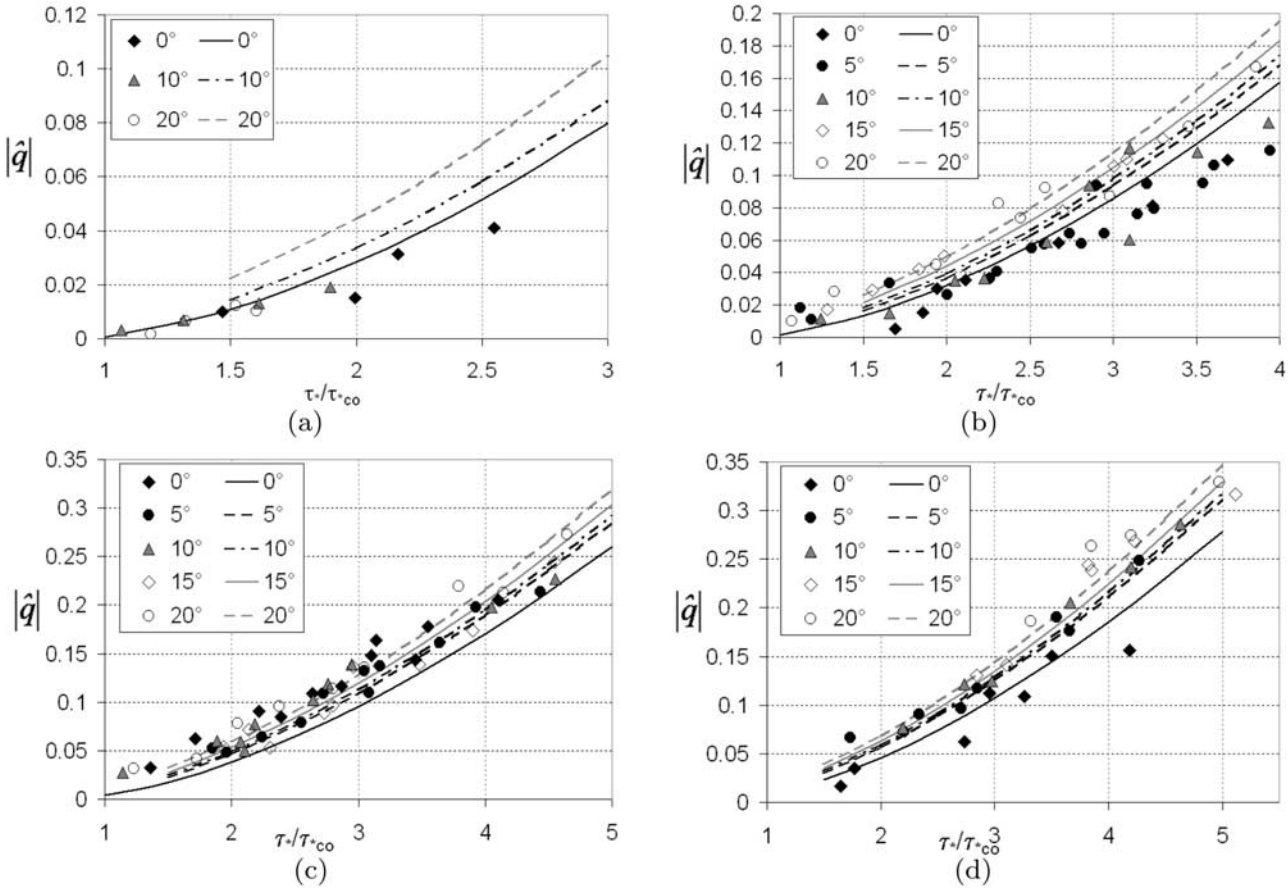

Figure 12. Dimensionless bed load transport rate: Experimental data (points) compared to the theoretical model of *Parker et al.* [2003] (lines) with (a) $\alpha = 1.72°$ and $\varphi = 0°$, 10°, and 20°; (b) $\alpha = 5°$ and = 0°, 5°, 10°, 15°, and 20°; (c) $\alpha = 10°$ and $\varphi = 0°$, 5°, 10°, 15°, and 20°; and (d) $\alpha = 15°$ and $\varphi = 0°$, 5°, 10°, 15°, and 20°.

areas of the cross section and to the local values of the Shields stress estimated in the measuring cross section.

[40] The measured values of the dimensionless bed load solid discharge are reported as a function of τ_*/τ_{*co} in Figure 12 and compared to the theoretical model proposed by *Parker et al.* [2003]. The results of the bed load transport rate are shown for the same longitudinal bed inclination (1.72°, 5°, 10° and 15°) and different lateral bed inclination φ. As expected, the local value of bed load transport rate turned out to be an increasing function of the applied Shields stress and of the local inclinations of the bed. In particular $|\hat{\mathbf{q}}|$ increases nonlinearly with α for a given φ, and with φ for a given α, the more so as τ_*/τ_{*co} increases. In the case of $\alpha = 1.72^o$ (Figure 12a), the experimental points show a weak dependence with the lateral inclination due to low values of τ_*/τ_{*co} investigated. In the other cases, both the experimental observations and the theoretical model have similar trends and the effect of the transversal inclination is confirmed to be not negligible, leading to the prediction of a considerable value of the transversal solid discharge in the case of steep lateral slopes.

[41] The dimensionless values of areal concentration of particles in motion, estimated from the measurements of bed load discharge and particle velocity, are reported in Figure 13 and compared with the theoretical values in terms of the dimensionless excess of residual shear stress divided by τ_{*co}. The trend of the data revealed that the relation between the areal concentration and the excess of residual stress is close to the linear one, thus confirming that the latter quantity may be taken as a measure of the entrainment capacity of the flow.

4.3. Test of the *Parker et al.* [2003] Model

[42] The observed values of the sediment transport rate, particle velocity and deviation angle are compared to the theoretical values as a whole (Figure 14). Considering Figure 14a, the observed values of the sediment transport rate are well predicted by the theoretical model, and the percentage of data that fall outside the lines ±30% of perfect agreement is 23%. The trend of the experimental values is well reproduced, while there are no systematic deviations from the calculated values.

[43] The particle velocity intensity is well predicted by the model (Figure 14b), and the percentage of data which fall outside the lines ±30% of perfect agreement is 4%, even though the model slightly underestimates the observed particle velocity around the threshold of motion and at lower values of the applied Shields stress, while it slightly overestimates the particle velocity intensity at higher Shields stress. This behavior may be due to the disk shape of the particles employed, whereas in the model sediment particles are modeled as spheres. The experimental scatter in

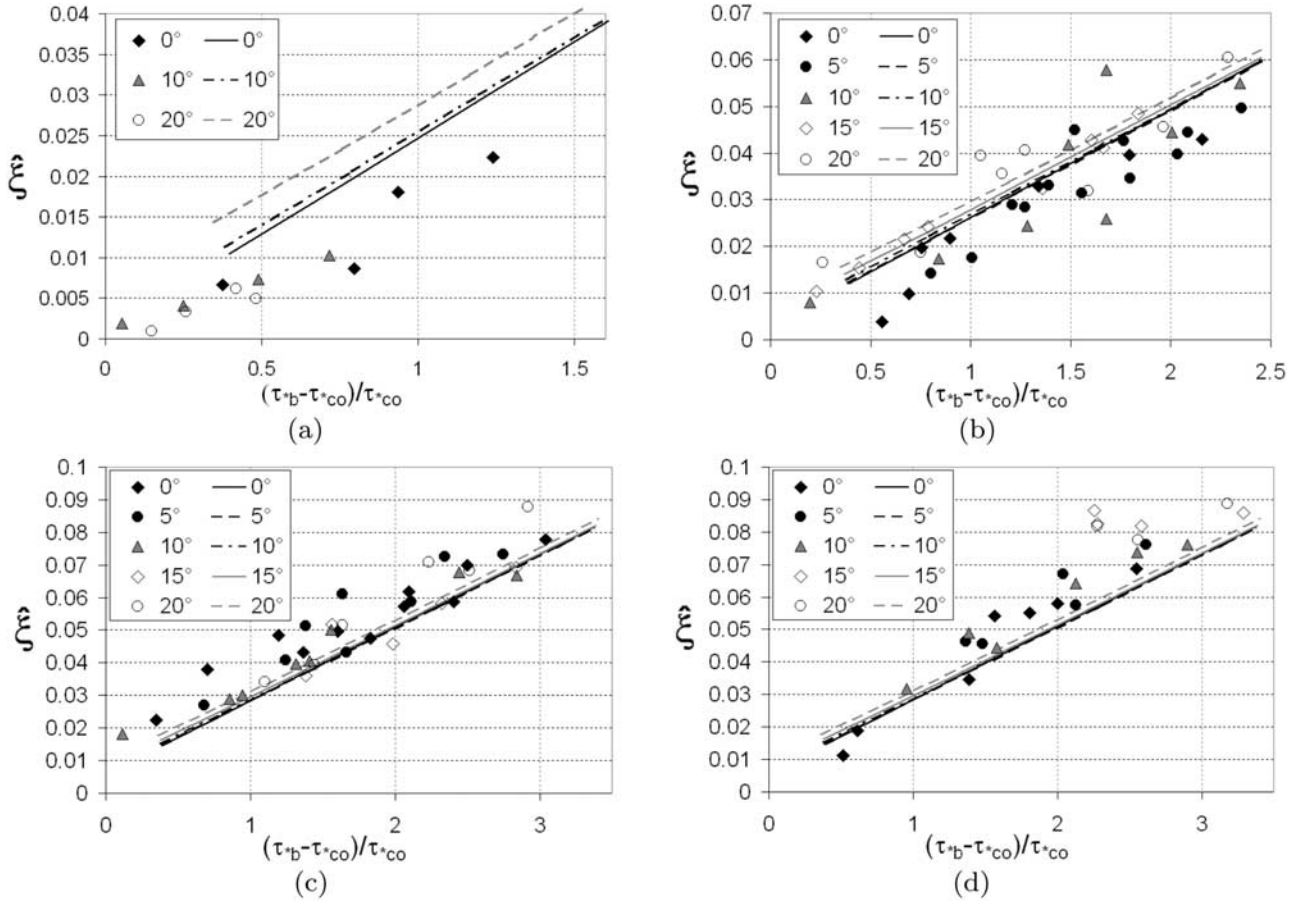

Figure 13. Dimensionless areal concentration: Experimental data (points) compared to the theoretical model of *Parker et al.* [2003] (lines) for (a) $\alpha = 1.72°$ and $\varphi = 0°$, 10°, and 20°; (b) $\alpha = 5°$ and $\varphi = 0°$, 5°, 10°, 15°, and 20°; (c) $\alpha = 10°$ and $\varphi = 0°$, 5°, 10°, 15°, and 20°; and (d) $\alpha = 15°$ and $\varphi = 0°$, 5°, 10°, 15°, and 20°.

the particle velocity data may also be responsible for the slightly different trend in data.

[44] At last, the deviation angle is well reproduced by the theoretical model (Figure 14c), and the percentage of data that fall outside the lines ±30% of perfect agreement is 14%. The comparison of observed and calculated values reveals that the deviation angle is better predicted at lower values, while at higher values the observations are overestimated by the model. This may be partially due to the difficulties in the estimation of the deviation angle, which is naturally ranging over a wide interval of values due to the irregular surface roughness of the nonerodible bed, and especially when τ_*/τ_{*co} is rather low and the particles experiences large angle of deviation.

[45] In order to obtain the best agreement of the theoretical model with the experimental values, a tuning of the main input parameters of the model was performed: to this aim several simulations were carried out with different values of the drag coefficient, the dynamic friction coefficient and the ratio of lift to drag coefficient. In particular simulations were run for the following values of the parameters: $C_d = 0.2$, 0.4, 0.5; $C_l/C_d = 1$, 1.25, 1.5; $\mu_{do} = 0.2$, 0.3, 0.5.

[46] Results show that the reduction of the drag coefficient leads to an overestimation of the calculated values of the sediment transport rate and the particle velocity intensity; the deviation angle instead seemed to be only slightly affected by the drag coefficient. The best agreement with the theoretical values was found for $C_d = 0.4$. The dynamic friction coefficient revealed a rather small effect on the particle velocity intensity and a relevant effect on the deviation angle. These effects combined together have an influence on the sediment discharge and give evidence that the better agreement of observed and calculated values is when $\mu_{do} = 0.3$. The fitting of the ratio of lift to drag coefficients showed a more sensitive behavior for the sediment transport rate and the particle velocity intensity and a negligible effect on the deviation angle. The best agreement was in the case of $C_l/C_d = 1.25$. The test performed here clearly shows that the observed quantities are in general well captured by the theoretical model employing values of the main input parameters that are very much reasonable and in agreement with the literature.

5. Discussion

[47] As outlined in the results section, the experiments support the theoretical model of *Parker et al.* [2003] and give insight into the bed load transport phenomenon. Many researchers have developed linearized formulations for estimating bed load transport on beds that are only modestly

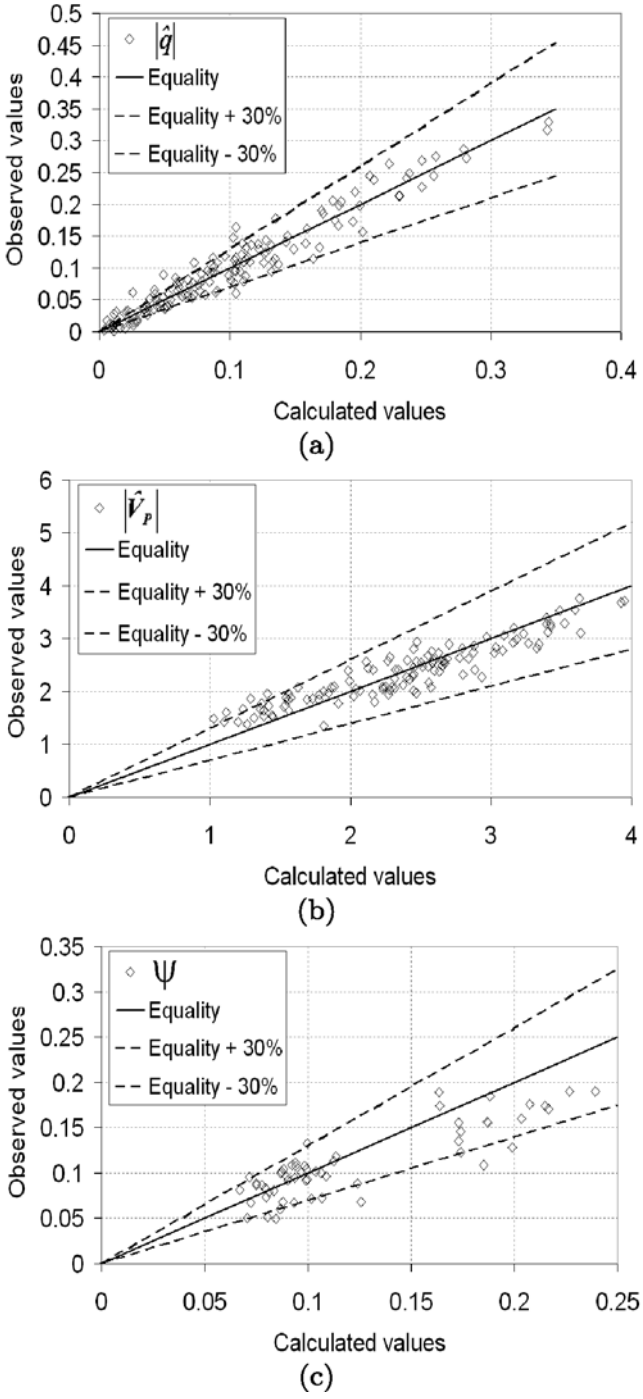

Figure 14. Observed versus calculated values with the *Parker et al.* [2003] model. Lines of perfect agreement (solid) ±30% (dashed) are also shown. (a) Dimensionless sediment transport rate. (b) Dimensionless particle velocity intensity. (c) Deviation angle.

sloping in an arbitrary direction, such that the following assumption holds:

$$(\sin\alpha, \sin\varphi, \sin\psi) \cong (\tan\alpha, \tan\varphi, \tan\psi) \tag{14}$$

$$(\cos\alpha, \cos\varphi, \cos\psi) \cong (1, 1, 1) \tag{15}$$

Under these conditions a linear dependence between $\tan\psi$ and $\tan\varphi$ is found [*Seminara et al.*, 2002] through the following:

$$\tan\psi = \lambda_o \sqrt{\frac{\tau_{*co}}{\tau_*}} \tan\varphi \tag{16}$$

where λ_o is the value of λ on a horizontal bed. Using the same assumption it is found that at lowest order of approximation $\hat{\xi}$ remains unchanged from that for a flat bed while the bed load transport vector takes the form

$$\hat{\mathbf{q}} = \hat{q}_o[\hat{\mathbf{s}} + \tan\psi(\hat{\mathbf{s}} \times \hat{\mathbf{n}})] \tag{17}$$

where $\hat{q}_o$ denotes the magnitude of the dimensionless Einstein bed load transport rate on a nearly horizontal bed and $\hat{\mathbf{n}}$ is the unit vector upward normal to the bed. Note that linear relationships between the lateral component of sediment discharge and the lateral bed slope have been derived by various authors [e.g., *Ikeda*, 1982a, 1982b; *Talmon et al.*, 1995].

[48] In Figures 15a–15c the observed values are compared to the estimated values from the linear approximation of *Parker et al.*'s [2003] model for the bed load transport intensity, the particle velocity intensity and the deviation angle. In the case of $|\hat{\mathbf{q}}|$ it appears that the linear formulation greatly underestimates observed values, especially when τ_*/τ_{*co} is high; in the case of $|\hat{\mathbf{V}}_p|$, the linear formulation provides similar, although consistently smaller, values. The major discrepancies are found for the deviation angle: the linear formulation predicts values about 2 times smaller than the observed ones. The implication of these findings is that the linear formulations do not generally provide an enough accurate description of gravitational effects on sediment transport both in terms of intensity and direction. The general good agreement of the experimental data with the *Parker et al.* [2003] model (Figure 14) suggests the need to incorporate this model in any morphodynamic scheme in order to reproduce the complex patterns of a natural river. In particular, some useful applications may be provided in the modeling of the morphodynamic patterns that show high values of the local bed slopes, such as in the case of braided rivers, steep mountain streams and gravel bed rivers.

[49] The experimental results presented here confirm the physical basis that is underneath the entrainment formulation, which overcomes the limitations imposed by the Bagnold's constraint, and open important issues on how they can be transferred in the case of an erodible bed with respect to the observed dynamics of bed load particles and the role played by coherent and semicoherent flow and grain structures.

[50] With regard to the dynamics of bed load particles, many authors found that the dominant mode of sediment movement is associated with a saltation mechanism, whereas rolling and sliding are much less common [e.g., *Bagnold*, 1973; *Fernandez Luque and van Beek*, 1976; *Nino and Garcia*, 1994a]. This is also in agreement with the experimental observations of *Abbott and Francis* [1977], who showed the occurrence of the rolling-sliding and saltation modes as a function of the so-called stage T, defined as the ratio τ_*/τ_{*c}. In particular, it clearly emerged that the rolling-sliding mode prevailed (about 60% of the

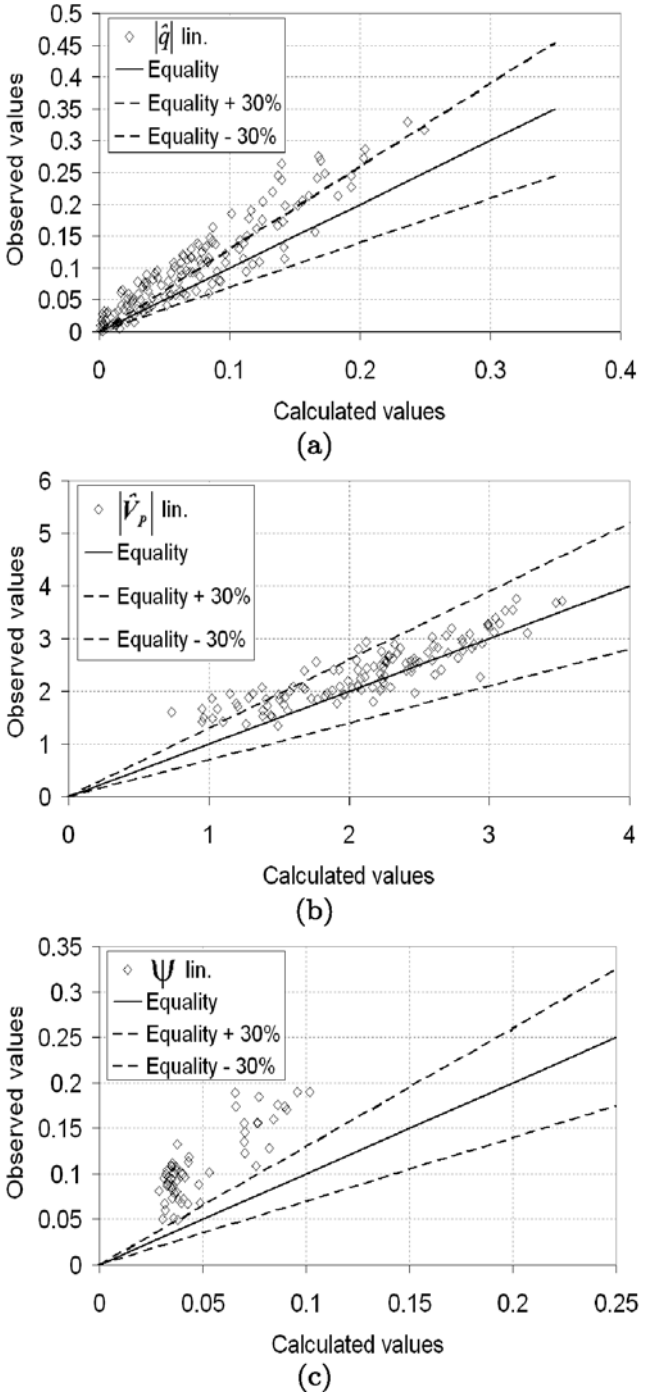

Figure 15. Observed versus calculated values using the linear approximation of the *Parker et al.* [2003] model. Lines of perfect agreement (solid) ±30% (dashed) are also shown. (a) Dimensionless sediment transport rate. (b) Dimensionless particle velocity intensity. (c) Deviation angle.

total time spent in transport) at threshold, then decreased rapidly (20% at $T = 1.4$) and practically disappeared as T reached a value near 3. Qualitatively similar field observations have been reported by *Drake et al.* [1988]. In the present work, an indirect estimate of the saltation mode in the performed experiments was given by the thickness of the saltation layer, which was assumed as the near-bed region where the particles were transported mainly as bed load: the latter layer thickness was estimated around 2–4 times the particle diameter by means of particle velocity profile and visual observations, which clearly indicated that particles were not only rolling and sliding over the bed, but also saltating.

[51] The entrainment of bed load particles is related to the spatial and temporal frequencies and the intensity of near-wall turbulent events (sweeps and inward interactions) [*Drake et al.*, 1988]. How these structures are affected by the mobile character of the bed is not obvious. However, since the experimental results interpret the findings of other authors in the case of bed load transport on a movable bed [*Fernandez Luque and van Beek*, 1976; *Nino and Garcia*, 1994a], the effect played by the nonerodible character of the bed on the coherent and semicoherent flow structure seems to be of the second order, at least in the context of the comparison for longitudinally sloping only bed. Another issue is related to the semicoherent grain structures, such as small-scale cluster bed forms, which seem to form in the range of low values of the applied Shields stress and in the case of heterogeneous sediment [*Hassan and Church*, 2000; *Lawless and Roberts*, 2001; *Strom et al.*, 2004]. These microforms alter the local flow turbulent structure, creating a three-dimensional flow field capable of influencing the erosion, transportation and deposition of other grains. How these phenomena are related to the bed load transport modeling is still under investigation.

6. Conclusions

[52] The present contribution is devoted to better understand the mechanism of bed load transport when transversal and longitudinal slopes are not negligible and in the case of low values of the applied Shields stress. Experiments aimed to study the particle dynamics and bed load transport on arbitrarily sloping beds at low Shields stress have been carried out. The effects of steep bed slope on bed load transport dynamics are investigated to test the validity of the theoretical model proposed by *Parker et al.* [2003] and are compared with the available experimental data from other sources in the case of a longitudinally tilted bed only [*Abbott and Francis*, 1977; *Fernandez Luque and van Beek*, 1976; *Nino and Garcia*, 1994a, 1994b]. From the authors' knowledge, no experiments in the case of a transversally tilted fixed bed in a water flume are available in the literature.

[53] The experiments were focused on the bed load transport rate at the equilibrium condition, flow velocity profiles and particle velocity measurements through a laser Doppler anemometer. Also, an image analysis technique was employed to estimate the particle velocity in terms of intensity and direction. The average concentration of sediment in motion was estimated from the previous quantities.

[54] The experimental data of particle velocity, concentration of particles in motion and bed load transport rate are in good agreement with the theoretical model proposed by *Parker et al.* [2003]. The measured deviation angle of particle velocity from the direction of the bed shear stress due to the transversal bed inclination is shown to be of the same order of magnitude as the theoretical one as well as a function of the applied shear stress and of transversal inclination, while the velocity intensities acquired with

images and laser techniques show similar values and errors. The experimental results of the bed load transport show that the intensity of bed load transport increases with the applied Shields stress much faster than predicted by the linear formulations in the case of a bed with negligible slope, giving evidence that the effect of gravity becomes particularly important when the downslope gravitational force has a component normal to the streamwise direction. In this case, the transversal downslope component of the particle velocity and bed load transport, which are predominantly directed in the streamwise direction, cannot be neglected.

[55] The above findings suggest that the application of a linearized model for sediment transport can lead to great underestimation of the bed load transport intensity and direction. This feature may play an important role in many phenomena for which the ability to predict a vectorial bed load transport rate up to the angle of repose of sediment is crucial, such as bank erosion, bed topography in river bends, sediment sorting and stream braiding.

[56] **Acknowledgments.** The authors are grateful to E. Paris, University of Florence (Italy), for his valuable comments and suggestions. G. Rovito and S. Carotti are acknowledged for the help in collecting the experimental data, and A. Lamberti, University of Bologna (Italy), is acknowledged for supplying the laser Doppler anemometer. The writers are also very grateful for the helpful comments provided by Marwan A. Hassan and an anonymous reviewer. This work has been developed within the framework of the National Project cofunded by the Italian Ministry of University and of the Scientific and Technological Research and by the University of Florence (COFIN 2001) "Morphodynamics of fluvial networks"; the authors also received financial support from CERAFRI (Center of Research and Advanced Education for Hydrogeological Risk Prevention).

References

Abbott, J. E., and J. R. D. Francis (1977), Saltation and suspension trajectories of solid grains in a water stream, *Philos. Trans. R. Soc. London, Ser. A*, *284*, 225–254.

Adrian, R. (1991), Particle-imaging techniques for experimental fluid mechanics, *Annu. Rev. Fluid Mech.*, *23*, 261–304.

Ashida, K., and M. Michiue (1972), Study on hydraulic resistance and bedload transport rate in alluvial streams, *Trans. Jpn. Soc. Civ. Eng.*, *206*, 59–69.

Bagnold, R. A. (1956), The flow of cohesionless grains in fluids, *Philos. Trans. R. Soc. London, Ser. A*, *249*, 235–297.

Bagnold, R. A. (1973), The nature of saltation and "bed-load" transport in water, *Philos. Trans. R. Soc. London, Ser. A*, *332*, 473–504.

Drake, T. G., R. L. Shreve, W. E. Dietrich, P. J. Whiting, and L. B. Leopold (1988), Bedload transport of fine gravel observed by motion-picture photograpy, *J. Fluid Mech.*, *192*, 193–217.

Engelund, F., and J. Fredsoe (1976), A sediment transport model for straight alluvial channels, *Nord. Hydrol.*, *7*, 293–306.

Fernandez Luque, R., and R. van Beek (1976), Erosion and transport of bedload sediment, *J. Hydraul. Res.*, *14*(2), 127–144.

Hassan, M. A., and M. Church (2000), Experiments on surface structure and partial sediment transport on a gravel bed, *Water Resour. Res.*, *36*(7), 1885–1895.

Hu, C., and Y. Hui (1996), Bed-load transport. I: Mechanical characteristics, *J. Hydraul. Eng.*, *122*(5), 245–254.

Ikeda, S. (1982a), Incipient motion of sand particles on side slopes, *J. Hydraul. Div.*, *108*(1), 95–114.

Ikeda, S. (1982b), Lateral bed load transport on side slopes, *J. Hydraul. Div.*, *108*(11), 1369–1373.

Lawless, M., and A. Roberts (2001), Three-dimensional flow structure around small-scale bedforms in a simulated gravel-bed environment, *Earth Surf. Processes Landforms*, *26*, 507–522.

Lee, H. Y., Y. H. Chen, J. Y. You, and Y. T. Hui (2000), Investigations of continuous bed load saltating process, *J. Hydraul. Eng.*, *126*(9), 691–700.

Nino, Y., and M. Garcia (1994a), Gravel saltation: 1. Experiments, *Water Resour. Res.*, *30*(6), 1907–1914.

Nino, Y., and M. Garcia (1994b), Gravel saltation: 2. Modeling, *Water Resour. Res.*, *30*(6), 1915–1924.

Nino, Y., and M. Garcia (1998), Experiments on saltation of sand in water, *J. Hydraul. Eng.*, *124*(10), 1014–1025.

Papanicolaou, A., P. Diplas, M. Balakrishnan, and C. Dancey (1999), Computer vision technique for tracking bed load movement, *J. Comput. Civ. Eng.*, *13*(2), 71–79.

Parker, G., G. Seminara, and L. Solari (2003), Bedload at low Shields stress on arbitrarily sloping beds: Alternative entrainment formulation, *Water Resour. Res.*, *39*(7), 1183, doi:10.1029/2001WR001253.

Sekine, M., and M. Kikkaua (1992), Mechanics of saltating grains, *J. Hydraul. Eng.*, *118*(4), 536–558.

Seminara, G., L. Solari, and G. Parker (2002), Bed load at low Shields stress on arbitrarily sloping beds: Failure of the Bagnold hypothesis, *Water Resour. Res.*, *38*(11), 1249, doi:10.1029/2001WR000681.

Strom, K., A. N. Papanicolaou, N. Evangelopoulos, and M. Odeh (2004), Microforms in gravel bed rivers: Formation, disintegration, and effects on bedload transport, *J. Hydraul. Eng.*, *130*(6), 554–567.

Talmon, A. M., M. C. L. M. Mierlo, and N. Van Struiskma (1995), Laboratory measurements of the direction of sediment transport on transverse alluvial-bed slopes, *J. Hydraul. Res.*, *33*, 495–517.

Wiberg, P. L., and J. D. Smith (1985), A theoretical model for saltating grains in water, *J. Geophys. Res.*, *90*, 7341–7354.

Wiberg, P. L., and J. D. Smith (1989), Model for calculating bedload transport of sediment, *J. Hydraul. Eng.*, *115*(1), 101–123.

S. Francalanci, CERAFRI, Via XI Febbraio, I-55040 Retignano di Stazzema, Lucca, Italy. (simona.francalanci@dicea.unifi.it)

L. Solari, Department of Civil and Environmental Engineering, University of Florence, Via S.Marta 3, I-50139 Florence, Italy. (luca.solari@dicea.unifi.it)